Front. Struct. Civ. Eng. 2023, 17(10): 1443–1464
https://doi.org/10.1007/s11709-023-0932-7

RESEARCH ARTICLE

Dynamic performance of submerged floating tunnel with different mooring styles subjected to anchor cable failure

Zhiwen WU[a*], Chuhan ZHANG[a], Liwang MOU[a], Guoxiong MEI[a*], Ankit GARG[b,c]

[a] *College of Civil Engineering and Architecture, Guangxi University, Nanning 530004, China*
[b] *Department of Civil Engineering, L.N. Gumilyov Eurasian National University, Nur-Sultan 010000, Kazakhstan*
[c] *Guangdong Engineering Center for Structure Safety and Health Monitoring, Shantou University, Shantou 515063, China*
[*] *Corresponding authors. E-mails: wuzhiwen20031985@163.com; meiguox@163.com*

ABSTRACT Submerged floating tunnels (SFTs) are novel structures for transportation across long- and deep-strait regions. Owing to severe wave and current excitation as well as the effects of underwater structures and corrosion, the risk of local anchor cable failure is high, which can result in the progressive failure of the entire structure. In this study, experimental and numerical investigations are conducted to analyze the dynamic behavior of an SFT with different mooring styles under local cable failure. A custom-designed cable failure device and the birth-and-death element method are used to simulate cable failure (i.e., progressive failure) via experiments and numerical simulation, respectively. A physical-scale segmental model of an SFT with different mooring styles under anchor cable failure is developed in this study. A segmental and entire-length mathematical model is developed using the ANSYS program to perform the numerical simulation. The results of the segmental numerical and experimental models indicate good agreement. The dynamic response of an SFT with different mooring styles under cable failure is comprehensively investigated by investigating the effects of key parameters (wave period, buoyant weight ratio, and cable failure mechanism). Moreover, the progressive failure of the SFT under cable failure is investigated via a segment model test and a numerical simulation of its entire length. The present study can serve as a reference for the safer designs of the SFT mooring style.

KEYWORDS dynamic behaviors, submerged floating tunnel, cable failure, mooring style, progressive failure

1 Introduction

A submerged floating tunnel (SFT) is a novel structure for transportation across long and deep strait regions [1]. A typical SFT system comprises primarily a tube suspended at a certain depth underwater, anchor cables that limit the excessive displacement of the tube, deep-water foundations, and revetment structures connecting both ends [2]. The SFT offers prominent advantages over classical traffic structures across rivers, lakes, and seas. The tunnel does not significantly affect the surrounding natural environment and can be operated under all weather conditions; in fact, it is not subjected to complex weather conditions such as tsunamis, storms, heavy rains, and fogs [3,4]. Therefore, SFTs have garnered increasing attention from scholars and engineers.

The mooring system is the key component of the SFT, which supports most of the applied loading to the entire structure, and the failure of the mooring system in a hostile environment will destroy the SFT. Therefore, the dynamic performance of the SFT mooring system under oceanic loading has received considerable attention from scholars. Lu et al. [5] investigated the effect of the vertical excitation of a floating system structure on the relaxation of a mooring system. Seo et al. [6] investigated wave loads on the mooring system of an elliptical SFT. Furthermore, they utilized Morison's equation to estimate wave loads composed of inertia and drag forces. Cantero et al. [7] analyzed the stability of SFT mooring cables under parameter excitation and investigated the effect of

Article history: Received May 17, 2022; Accepted Nov 11, 2022

parameter resonance on vertical mooring tension. Naik et al. [8] evaluated the static and dynamic responses of an SFT mooring system under hydrodynamic loading. Luo et al. [9] investigated the displacement response of the mooring system of an SFT with a flexible boundary under an explosive load. Chen et al. [10] presented a numerical model of the mooring system of an SFT and investigated the characteristics of wave–tunnel interactions for different hydrodynamic parameters. Xie and Chen [11] proposed a new mathematical model to analyze the dynamic response of the mooring system of an SFT under the action of sine and seismic waves.

In most related previous studies, mooring cables and SFT responses are primarily analyzed. However, studies that investigate the effect of mooring style on SFT performance are few. A favorable mooring style for the SFT must not only ensure its survivability, but also must consider its effects on the motions and load characteristics. Furthermore, the moorings should be easy to monitor and maintain while minimizing the material and installation costs. Thus, the effect of mooring styles on the dynamic response of SFTs must be investigated as the findings can provide guidance for selecting the most suitable mooring styles and for reducing the project cost without affecting its dynamic performance. To the best of our knowledge, studies regarding the dynamic performance of SFTs with different mooring styles are rare. Lee et al. [12] evaluated the dynamic performance of a short-, rigid-, and free-end SFT section with vertical and inclined mooring cable configurations. Liu et al. [13] investigated the effect of the inclined angle of an anchor cable on the motion characteristics of an SFT under wave action.

In addition, as the key bearing member of the mooring system, cables have been widely used for SFTs to transfer tension loads between the tube and foundations. These cables are exposed to corrosion, fatigue, and abrasion, which deteriorate their section and resistance capacities. Cable failure events cannot be completely avoided owing to various hazards such as severe waves and current excitations, natural disasters (e.g., earthquakes, submarine landslides, and tsunamis), the effect of underwater structures, long-term corrosion and fatigue, and structural degradation. Once cable failure occurs, distinct response variations and internal force redistribution of the SFT will occur, and the entire structure may fail progressively. To prevent the cable failure hazard from becoming disastrous, the subsequent hydrodynamic behaviors and progressive failure of SFTs under cable failure, as well as the corresponding prevention and countermeasures, should be emphasized. Xiang et al. [14] used the dynamic amplification factor and coefficient to estimate the effects of cable failure. They developed numerical and test models to investigate the dynamic responses and mechanical behaviors of an SFT subjected to abrupt anchor-cable failure. However, the combination of both wave and current excitations was not considered in existing simulation methodologies. In the experimental SFT model, cable failure was not triggered by the minimum breaking load of the cable. Instead, it was induced by cutting one cable using a sharp wire cutter at the beginning of the dynamic cable-breaking test, which implies that the subsequent failure behavior of the remaining cables cannot be simulated. Moreover, the progressive failure of SFTs induced by cable failure has not been considered in previous studies.

Recently, some scholars have conducted numerical simulations and experiments to simulate the cable (or other local structures) failure of structures, such as cable-stayed bridges, suspension bridges, and offshore wind turbines. Zhou and Chen [15] conducted a numerical investigation of cable failure events in long-span cable-stayed bridges under stochastic traffic and wind conditions. Minaei et al. [16] investigated the global structural dynamics of a cable-stayed structure subjected to cable failure and confirmed the cable failure equivalent force with respect to time. Wu et al. [17] developed a modified series–parallel system and conducted a nonlinear dynamic analysis of a self-anchored suspension bridge subjected to an abrupt failure of a hanger. Bae et al. [18] investigated the dynamic performance of a floating offshore wind turbine with mooring line failure by performing numerical simulations.

In this study, experimental and numerical investigations are conducted to analyze the dynamic behavior of an SFT with different mooring styles under local cable failure. A custom-designed cable failure device and the birth-and-death element method are used to simulate cable failure events in the experiment and numerical simulation, respectively. A physical-scale segmental model of an SFT with different mooring styles under wave and current loading is performed in a wave–current flume. Based on the calculation theories of the fully dynamic simulation analysis method and cable dynamics theory, a corresponding segmental numerical model and an entire-length numerical model are developed using the ANSYS program. Subsequently, a comparison is performed to verify the consistency and availability of the numerical and experimental results. The dynamic response of an SFT with different mooring styles under cable failure is comprehensively investigated based on different key parameters, such as the wave period, buoyant weight ratio (BWR), and cable failure mechanism. Moreover, the progressive failure phenomena of SFTs under cable failure are investigated via a segment model test and a numerical simulation of their entire length.

2 Experimental model description

2.1 Wave–current flume and its instrumentation design

In the experiment, an SFT scheme for crossing Funk Bay was used as a prototype [19]. Based on the dimensions

and wave–current generation ability of the wave–current flume, previous studies [20–22], and the similarity theory, the scaled segment model of the SFT was designed with a geometrical scale λ of 1 : 100. The main parameters of the SFT model are listed in Table 1, and their environmental parameters are listed in Table 2.

Based on previous studies [23,24], three typical mooring styles for SFTs were adopted in the current study, as shown in Figs. 1(a)−1(c). A detailed illustration of the test setup of the SFT model is shown in Fig. 1(d). The physical model primarily comprises a tunnel tube and 18 cables exhibiting the aforementioned three typical mooring styles, which were fabricated using plexiglass and steel wire ropes, respectively. The mooring style 1 is set as a typical case, its six external cables (numbered as Nos. 1–6) were apportioned into three pairs. For mooring styles 2 and 3, the six internal cables were numbered as Nos. 7–12.

The present experiment was performed in the wave–current flume, which measured 30 m long, 1.5 m wide, and 1.5 m deep. At the end of the flume, a push-board wave maker was used to generate the desired incident waves, and the tilt-type wave absorber was used to prevent the wave reflection from adversely affecting the test results. A uniform and steady current can be generated and ensured using a large-scale pump. A custom-designed circulating loop and a porous guide plate was installed at the inlet and outlet of the flume, respectively. In wave–current tests, the wave maker and pump function independently. For each wave–current case, current was generated first to acquire a steady current velocity. Subsequently, the wavemaker system was activated to generate a solitary wave. When simulating cases of waves with currents, currents were introduced via the bed of the flume in front of the wavemaker [20,21,25]. The typical target and measured values of the water-level elevation in the time domain under different wave and current combinations is shown in Fig. 2.

Table 1 Main parameters of the tunnel tube and anchor cables

component	parameter	unit	value
tunnel tube	length	m	1.46
	segment length	m	0.6
	outer diameter	m	0.2
	elastic modulus	GPa	2.4
	density	$kg \cdot m^{-3}$	1.18
	BWR	–	1.5
anchor cables	elastic modulus	GPa	206
	diameter	m	0.002
	length of incline cables	m	1.06
	length of vertical cables	m	0.75
	length of crossover cables	m	1.26
	pretension	N	48.6 (mooring style 1)/ 44.7 (mooring styles 2 and 3)

Table 2 Environmental parameters

parameter	unit	value
water depth	m	1.0
wave height	m	0.03
wave period	s	0.5, 0.7, 0.9, 1.1, 1.3, 1.5, and 1.7
flow velocity	m/s	0.1
immersion depth	m	0.15

Based on previous studies [20–22], the experimental SFT model and its detailed connections between different tube components were designed, as shown in Figs. 3(a)–3(c). The tube body model was partitioned into three sections, i.e., two side sections measuring 0.6 m and a middle section measuring 0.2 m. The flange plate was set on the end of each tube via six bolt holes to connect different components. The middle section was designed to allow the installation of sensors in the barycenter of the tube body. To prevent water seepage, a water stop was fixed between the connections of the tube joints. Based on the connection between the general marine structure (e.g., the pipeline and immersed tunnel) and its anchor cable, the connection between the tube body and anchor cable in this study was set to a hinge joint [22], as shown in Fig. 3(d). The hinged connectors were attached at the connecting point of the SFT tube, and the anchor cables through the hinged connectors were secured by aluminum sets.

Based on previous studies [20,21], the pretention of the anchor cables was set between 45 and 50 N in the present experiment (see Table 1 for more details). Notably, the number of anchor cables are different for different mooring styles, and the pretensions of anchor cables between different mooring styles differ slightly under the same remaining buoyancy for the entire SFT.

Tensile force gauges were mounted above the water ends of the external cables to monitor the tension of the cables. The gauge contains a custom-designed monitoring device for cable tension tests and failure triggers (details are described in the following section). In this study, owing to limitations imposed by the experiment cost and duration, the dynamic performance of the internal decussate anchor cables under anchor cable failure was not investigated and analyzed comprehensively.

An inertial measurement unit was mounted at the center of gravity of the tube to monitor the rotation of the tube in the test. The displacement (sway, heave, and surge) of the tube was measured using a three-dimensional (3D) digital image correlation (DIC-3D) measurement device. In the DIC-3D measurement device, structural displacement is obtained by binocular cameras using the ray-tracing method, which is a non-intrusive technique for the high-

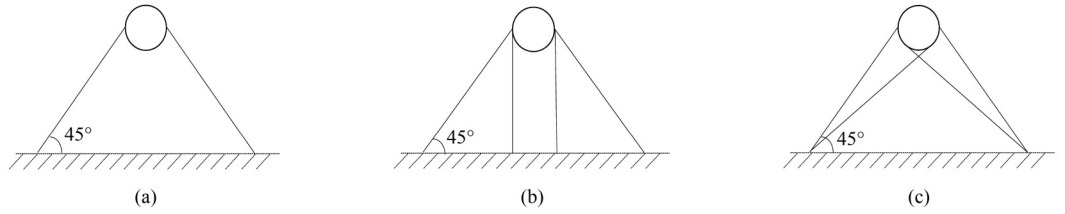

(a) (b) (c)

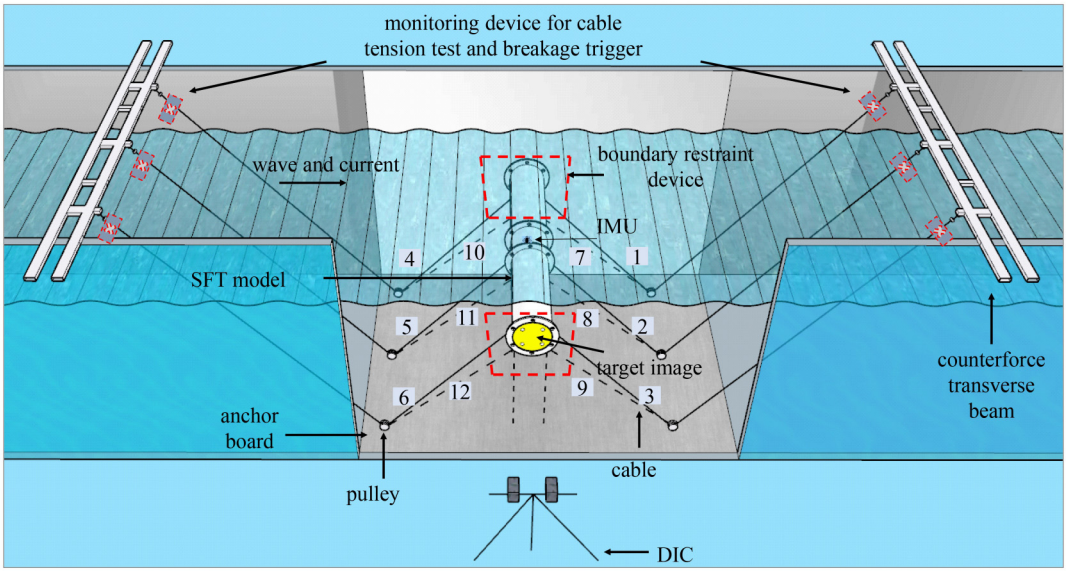

(d)

(e)

Fig. 1 Experimental setup of SFT model. (a) Mooring style 1; (b) mooring style 2; (c) mooring style 3; (d) schematic illustration of experimental setup; (e) main measuring equipment.

precision measurement of moving structures. In this study, a DIC-3D device was set directly in front of the tube, and four circinate tracker images were pasted on the surface of the front end of the tube (Fig. 1(e)). The tracker's movement trails were captured using cameras, which can convert 2D movement photographs of trackers to the 3D movement characteristics of the tube. The main measuring instruments used in this test are shown in Fig. 1(e). Restraint devices were installed between the support frame and each end of the tube to simulate the boundary condition of the tube.

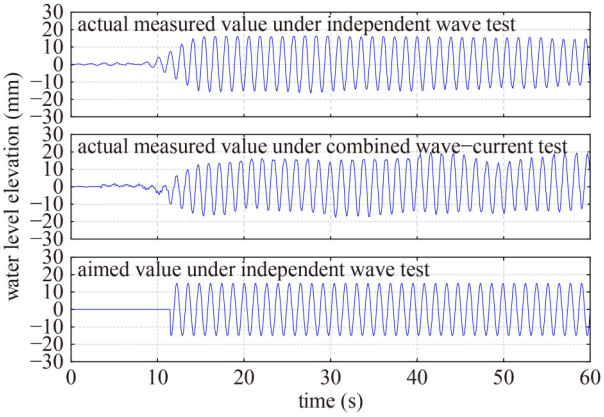

Fig. 2 Typical target and measured values of water-level elevation in time domain under different wave and current combinations (wave height = 30 mm, wave period = 1.3 s, and current velocity = 0.1 m/s).

2.2 Newly designed cable-breaking simulation device

To simulate cable failure, a custom-designed cable-breaking simulation device was used in this study (Fig. 4). The cable-breaking simulation device primarily comprised a turnbuckle, tensile force gauges, an electromagnet, an iron pan, and an external control circuit. The turnbuckle was connected to the counterforce transverse beam to adjust the cable tension. The tensile force gauges were used to measure the real-time tension of each cable and to control the magnetic loss of the electromagnet with the assistance of an external control circuit when the cable dynamic tension exceeded the presupposed threshold value. Once the electromagnet loses its magnetism, it becomes separated from the iron pan fixed in the cable, thereby allowing the experimental

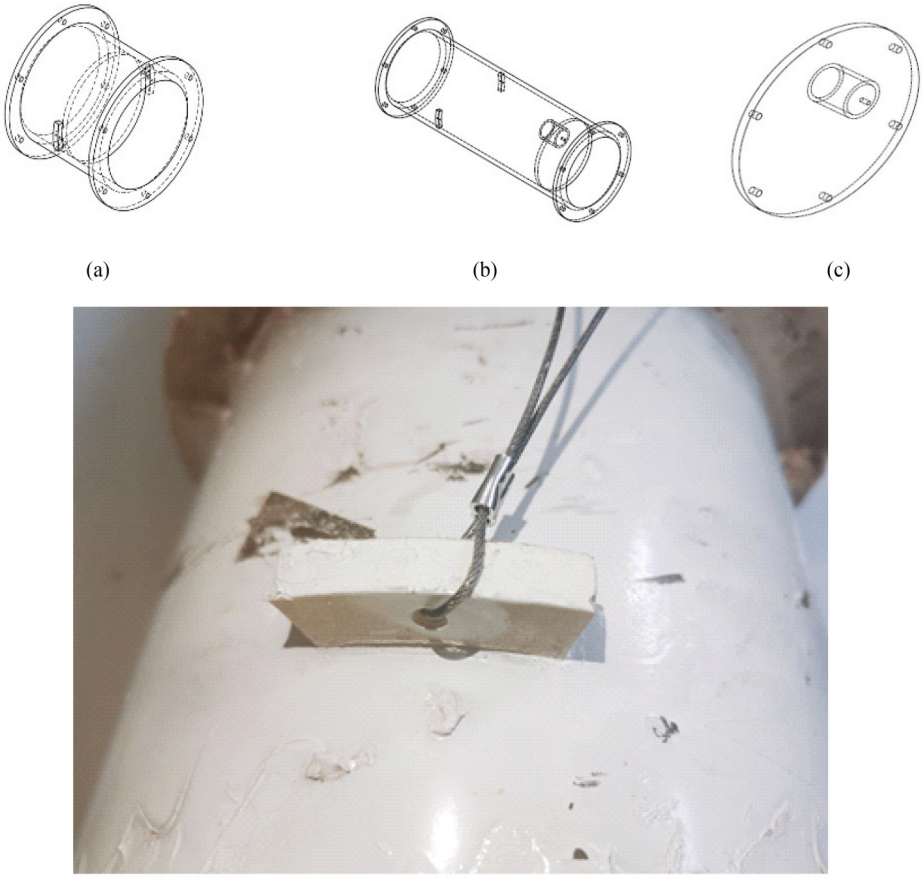

Fig. 3 Schematic illustration and photograph of SFT connection. (a) Intermediate section; (b) side of tube; (c) connection of tube; (d) details of connection between tube body and anchor cable.

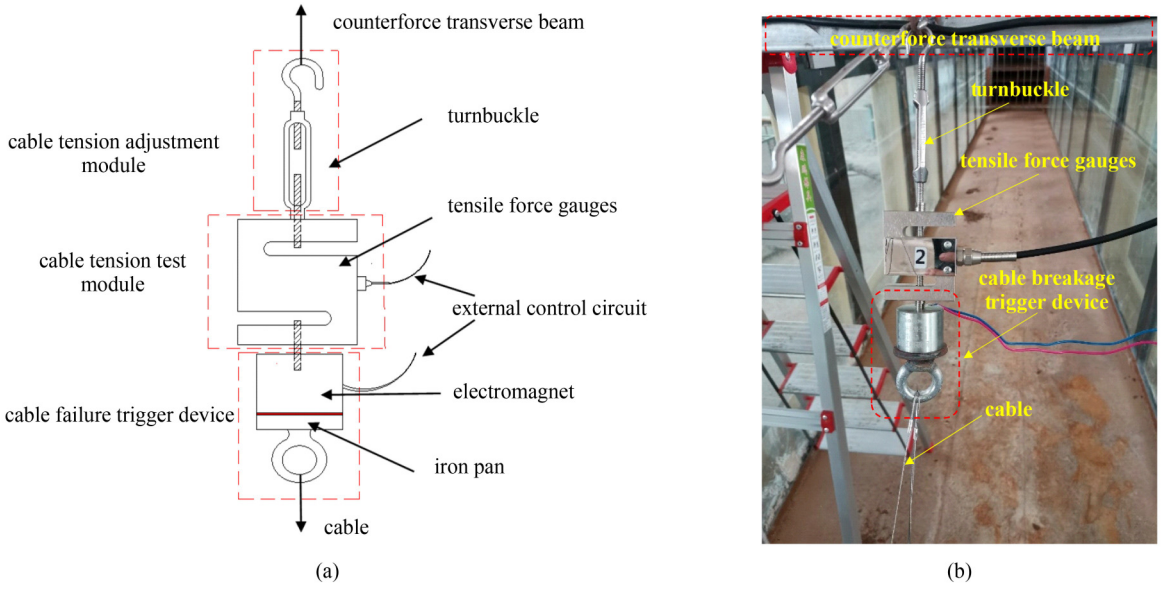

Fig. 4 Monitoring device for cable tension test and failure trigger. (a) Sketch; (b) image.

simulation of cable failure based on force control. Furthermore, cable failure based on timing control can be achieved using an external switch to control the magnetism of the electromagnet. Hence, cable failure can be simulated using force and timing controls. In summary, the conditions for triggering cable failure can be controlled by the cable tension or an external switch for different cases. Notably, the subsequent cable failure behavior of the remaining cables and the progressive failure of the SFT subjected to cable failure can be simulated using the failure device used in the current test.

2.3 Details of the boundary restraint device

Because of the dimensional limitations of the test flume, most test investigations are typically conducted on segmental SFT models, and both ends of the segmental tube are simulated based on a free constraint [6,26]. In actual conditions, the SFT is generally fixed to the rock stratum, the land foundation, or the artificial foundation in a shallow marine site. Thus, the restraint condition at both ends of the segmental tube can be regarded as a simply supported boundary when the entire length of the SFT model is considered. However, for the segmental SFT model, the restraint at its two ends was derived from the restraint of the adjacent tube segments. This restraint effect is complicated and governed by many factors, such as the span of the SFT, the location of the segmental tube at the SFT, the geometrical and material parameters of the tube, the mooring style, and the shore-connecting style. Thus, the boundary restraint condition of the segmental SFT model cannot be realistically simulated by considering both ends of the tube as free.

Based on previous studies [20,21,27], a specific boundary restraint device was designed in this study (Fig. 5). Spring-damping system sets were installed in four directions at one end of the tube. One end of the spring-damping system was linked to the tube, whereas the other

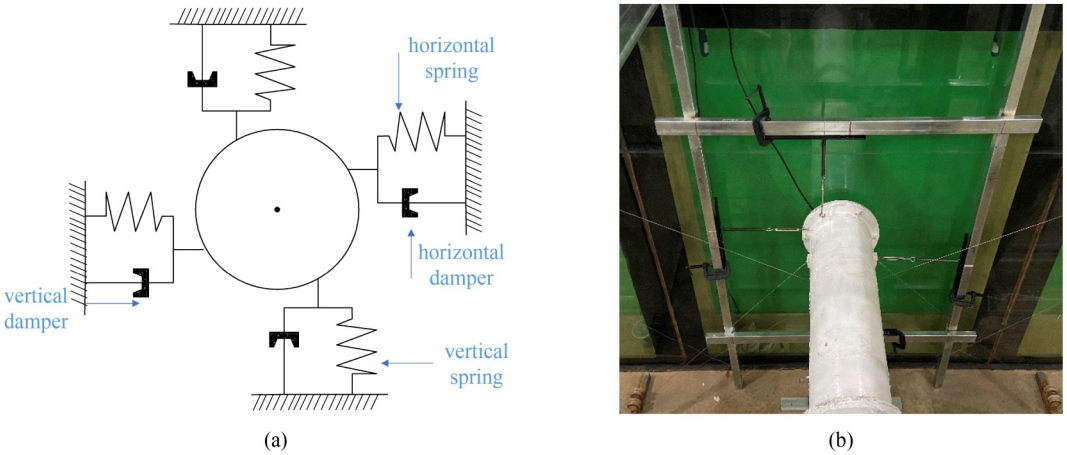

Fig. 5 Boundary restraint device. (a) Simulation scheme of boundary constraint; (b) photograph of boundary restraint device.

end was connected to the support structure. In this test, the sway, heave, and roll were the main motion directions of the SFT during the flume. Four horizontal springs and dampers installed at the two ends of the tube were used to simulate the stiffness and damping of the tube, respectively, in the sway direction. Similarly, four vertical springs and dampers at the two ends of the tube were used to simulate the stiffness and damping of the tube in the heave direction. In total, four sets of spring-damping systems were asymmetrically installed at the cross-section of the tube to provide an additional force to simulate the rotation stiffness in the roll direction of the segmental SFT model. A numerical link method was applied to connect the entire-length numerical model to the segment test model of the SFT. A segment model designed based on the abovementioned boundary restraint was used to reproduce the movement and stress state of the entire-length model. In the test, the parameters of the spring-damping system for the physical segment model were obtained by fitting the values from the entire-length numerical model. Notably, the parameter values of the boundary restraint were different for different test cases.

Based on previous studies [20,21], segmental and entire-length numerical simulation models were established to assess the validity of the boundary restraint device. More details regarding the comparison of the models are available in Refs. [20,21]. Based on the results, the boundary restraint device is acceptable, reasonable, and can provide a sufficiently accurate analysis of the hydrodynamic behaviors of the SFT.

2.4 Test case design for investigating effects of wave period and buoyant weight ratio

In the current test, the dynamic performance of an SFT with three mooring styles under cable failure was comprehensively investigated based on key parameters, such as the wave period and BWR. Furthermore, to investigate the progressive failure mechanism of the SFT for different mooring styles under cable failure, a specific failure case was established to trigger the progressive failure of the entire model. The details of this case are as follows: the breaking tensions of all cables were reduced to 75 N, and cable No. 5 was triggered to break at 30 s via a combination of timing control and force control methods. Notably, the cable-breaking simulation device was set on only the No. 5 anchor cable, and only the No. 5 cable outside the inclined anchor cable was broken in the test. It is noted that the cable-breaking simulation device is only set on No. 5 anchor cable, and only No. 5 outside inclined anchor cable is broken in this test. The main test design cases and their values are presented in Table 3. A photograph of the SFT is shown in Fig. 6.

Table 3 Test cases

parameter	value/description
regular wave height (cm)	3.0
regular wave period (s)	0.5, 0.7, 0.9, 1.1, 1.3, 1.5, and 1.7
current velocity (m/s)	0.1
wave and current direction (°)	0
BWR	1.3 : 0.2 : 2.1
cable failure mechanism	No. 5 cable failure; reducing the breaking tensions of all cables to 70 N; triggering No. 5 cable failure at 30 s

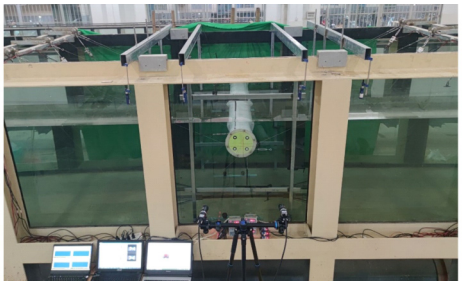

Fig. 6 Photograph of SFT test setup.

3 Numerical model for simulating progressive failure of cable and combination of wave and current excitation

3.1 Establishment of numerical model for SFT

AQWA, which is widely recognized as an effective hydrodynamic calculation software for simulating the wave–current interaction and hydrodynamic analysis for marine engineering structures, was used to establish the SFT model in this study. Hydrodynamic models were established using the hydrodynamic solver of AQWA based on 3D potential theory and the boundary element method. The assumptions of the theory are as follows: 1) the fluid flow is inviscid, incompressible, and irrotational; and 2) the amplitude of the waves is smaller than their length. The current in this test was assumed to be a uniform and steady, and its loads exerting on the SFT were calculated using the Morison equation. The fully coupled calculation method was used to consider the wave–current and fluid–structure interactions in the numerical simulation. Based on the calculation theories used in the fully dynamic simulation analysis method and cable dynamics theory, the present numerical model of the SFT was established using the LINE and Drift modules. The LINE module was used to define the geometrical and physical parameters of the tube, calculate the linear wave force in the frequency domain, and perform preliminary calculations for the following coupled analysis in the time domain using diffraction/

radiation hydrodynamic calculations. The Drift module is primarily used to define the wave–current loading coefficients, mooring constraints, and cable parameters. Furthermore, it is useful for conducting coupled dynamic analysis of SFTs under wave and current excitations in the time domain. The added mass and damping coefficient of the SFT can be obtained using the Green's function method in the frequency domain. The current force applied to the SFT was calculated using the Morison equation, and the inertia and drag coefficients in the equation were obtained based on DNV-RP-C205 [28]. The SFT tube was modeled using a PMAS element. The cable was modeled using the COMP/EACT component, and the catenary form of the cable was considered. For the segmental and entire-length models, 2 and 21 pairs of mooring cables were arranged along the SFT, respectively, and the interval of each pair of cables was 100 m. The numerical model was based on the original size of the SFT scheme for crossing Funk Bay.

3.2 Procedure for simulating cable failure

In this study, a full-dynamic natural simulation method and the birth-and-death element method were used to simulate cable failure numerically. During the simulation, the cable was first modeled as an elastic–plastic element, and then its yield strength and ultimate failure strength were specified. Its elastic–plastic characteristics were simulated using an isotropic hardening model. After the end of the dynamic calculation in each step, the stress on the cable was verified. As the cable stress exceeded its ultimate failure strength, the element of the cable was removed. Thus, the stress–strain state of the cable depends on its loading; therefore, the simulation of the entire cable failure process, from yielding to fracturing, is more realistic. In addition, the alternate load path method, which is primarily used in the dynamic calculation of large-span spatial structures, was applied to simulate the instant failure of cables via timing control. Using the abovementioned methods, the abrupt failure of the cables was achieved by adopting the LBRK command in ANSYS. Using the LBRK command, the cable failure time and ultimate failure strength can be defined to simulate cable failure via force control and timing control.

4 Validity assessment of numerical and experimental approaches

4.1 Comparison between numerical and experimental results

To determine the natural frequency of the segmental SFT model, experimental decay motion tests and numerical simulations were conducted in static water. Table 4 summarizes the simulated decay test results of the segmental SFT model for the three mooring styles. The measured and numerical values of the sway, heave, and roll motions appeared to agree well with each other. The two methods and models can be used to predict the subsequent dynamic performance and progressive failure behavior of SFTs under cable failure more accurately for field applications.

To further verify the consistency between the numerical and experiment results, the segment numerical models under different mooring styles were established using the ANSYS program (as shown in Fig. 7).

Figure 8 shows a comparison between the computed and measured time histories of 1) the dynamic responses of the tube and 2) the tension of cable of the SFT. To

Table 4 Natural period of segmental SFT model for three mooring styles

mooring style	test method	sway (s)	heave (s)	roll (s)
mooring style 1	experimental	1.10	0.25	1.40
	numerical	1.15	0.26	1.46
mooring style 2	experimental	0.46	0.18	0.45
	numerical	0.49	0.18	0.47
mooring style 3	experimental	0.45	0.21	0.43
	numerical	0.48	0.22	0.46

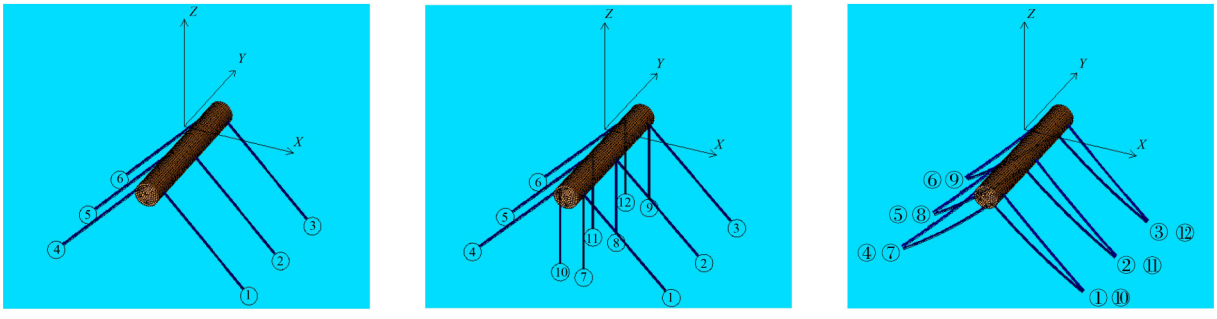

Fig. 7 Segment numerical models corresponding to SFT test models under different mooring styles. (a) Mooring style 1; (b) mooring style 2; (c) mooring style 3.

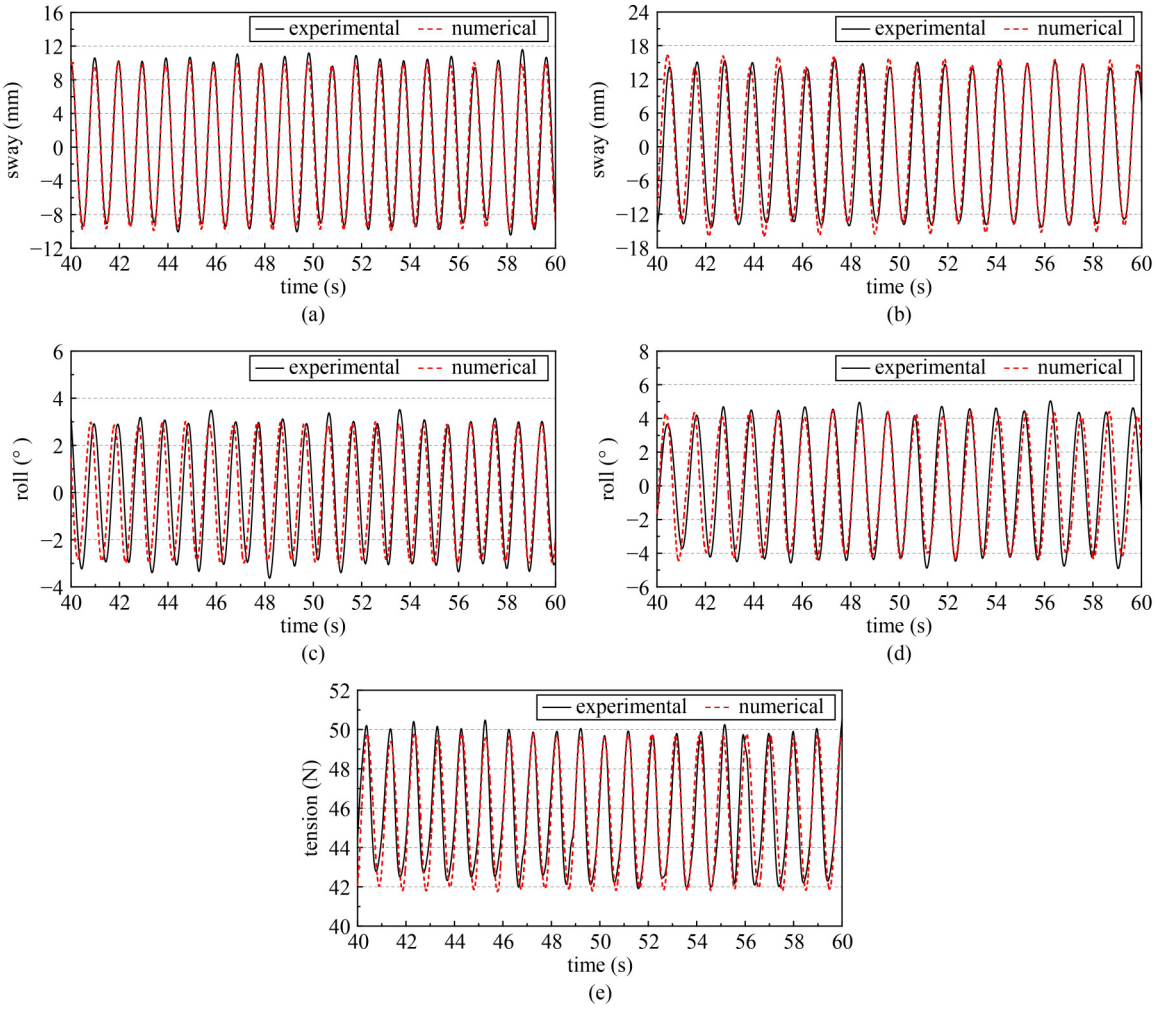

Fig. 8 Comparison of time histories of dynamic responses of tube and tension of cable between numerical and experimental results. (a) Sway (wave height = 3 cm; wave period = 1.1 s); (b) sway (wave height = 3 cm; wave period = 1.3 s); (c) roll (wave height = 3 cm; wave period = 1.1 s); (d) roll (wave height = 3 cm; wave period = 1.3 s); (e) tension of No. 5 cable (wave height = 3 cm; wave period = 1.1 s).

eliminate the effect of the initial transient behavior, the time histories for all the curves from 40 to 60 s were analyzed for the comparison. Based on observation, both the changes in the amplitudes and trends of the curves for the numerical and experimental results indicated high consistency, with a relative error of less than 5%. Only a few discrepancies were observed from the curves of the numerical and experimental results, which may be due to the uncontrollable factors in the test, e.g., the assembly error of the SFT model, the accuracy of the test devices, and the measuring error.

Figure 9 presents a comparison of the computed and measured maximum tensions of the No. 5 cable for different mooring styles. Generally, data from each measuring point agreed well with the numerically calculated values for different BWRs and mooring styles. Slight differences were observed, i.e., the maximum tension of the cable obtained from the test was slightly larger than that obtained from the numerical simulation. These differences might be caused by several factors, e.g., the tube–water coupling, the incomplete consideration of the effect of current on the tube in the numerical model, the installation error of the physical model, and the accuracy of the sensors. In both the computed and measured results, the maximum tensions of the No. 5 cable increased with the BWR. In addition, the tension of the cable for mooring style 1 was the largest among the mooring styles. This implies that the highest cable tension was maintained in mooring style 1 owing to the least number of cables used.

Additionally, some typical cases were considered for comparison to assess the efficacy of the test and numerical simulation for the SFT with cable failure (as shown in Fig. 10). Based on observation, the pattern of most of the test data was similar to that of the numerical simulation result. Furthermore, the overall trend of the curves obtained from the numerical and measured results was similar. As the wave period increased within the range of 0.5–1.3 s, the maximum tension of the cable for both the SFT with and without cable failure increased in

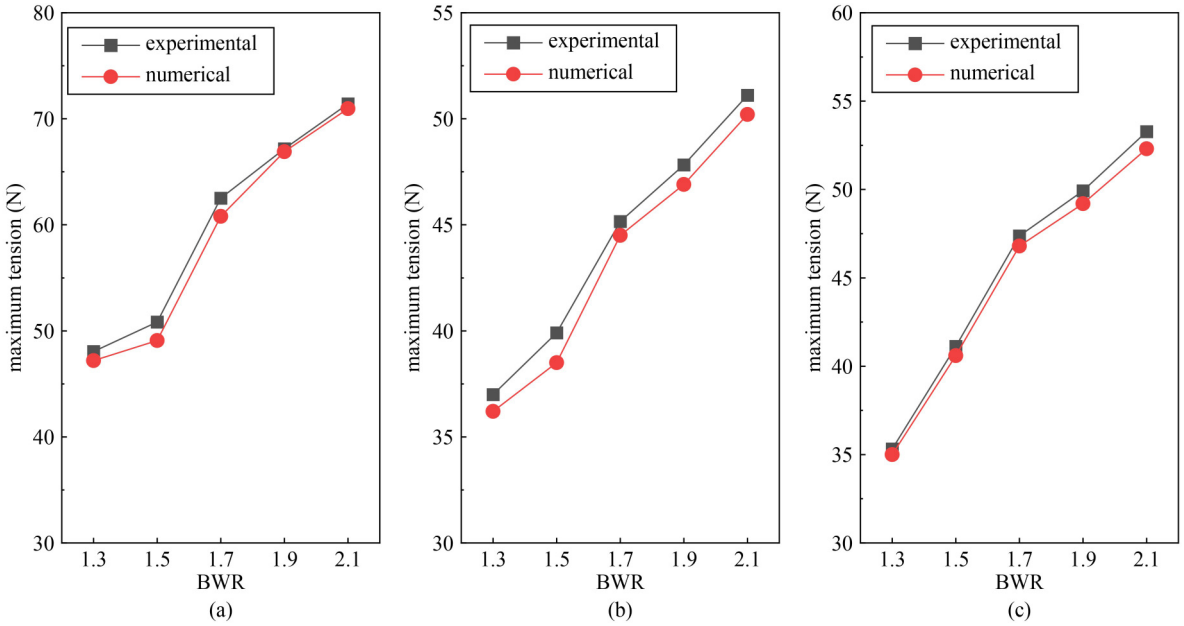

Fig. 9 Comparison of maximum tensions of No. 5 cable for different mooring styles between numerical and experimental results. (a) Mooring style 1; (b) mooring style 2; (c) mooring style 3.

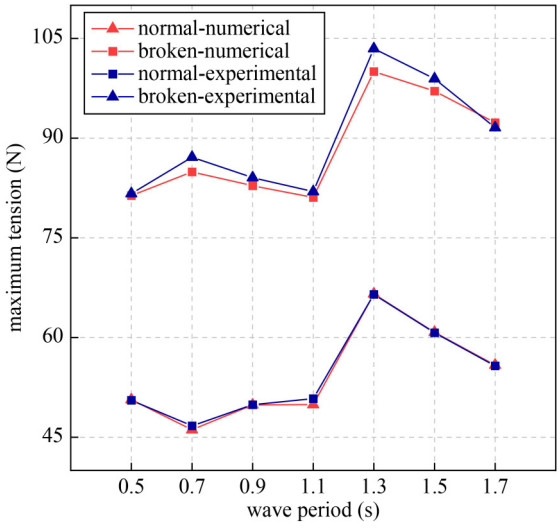

Fig. 10 Comparison of maximum tension of No. 4 cable between numerical and experimental models of SFT with and without No. 5 cable failure (wave height = 3 cm).

general and reached a maximum value at approximately 1.3 s, after which the value attenuated. In addition, the variation in the cable tension due to cable failure was significant, which implies that the cable failure inevitably increased the burden of the remaining cables, in particular for the case with a wave period of 0.7 s. This implies that, under cable breakage, the failure risk of the remaining cables is more severe when the SFT is in the resonance point between the tube motion and wave–current action.

The comparison results presented above indicate that the proposed experimental and numerical models are reasonable and acceptable. Thus, that these two methods are feasible for investigating the dynamic response of SFTs of different mooring styles with cable failure.

4.2 Reasonability assessment of excluding measurement and analysis inside decussate anchor cables under cable failure

To simplify the experiment, the measurement and analysis for the inside of decussate anchor cables under cable failure were excluded in the test. Two segmental numerical models with mooring styles 1 and 2 were established using the previously mentioned method to assess the reasonability of this simplification. A comparison of the tension change between the internal and external inline anchor cables under cable failure based on the additional numerical calculation is shown in Fig. 11.

As shown in Figs. 11(a) and 11(b), the tension amplitude and increment of the inside decussate anchor cables under cable failure are lower than those of the outside inline anchor cables, i.e., the effect of the inside decussate anchor cables is insignificant under cable failure. Thus, excluding the measurement and analysis for the inside of the decussate anchor cables under cable failure in the test is reasonable and acceptable for this study.

5 Results and discussions of segmental experiment model

5.1 Experimental results for typical case with different mooring styles

In the typical test case (wave height = 3 cm, wave period =

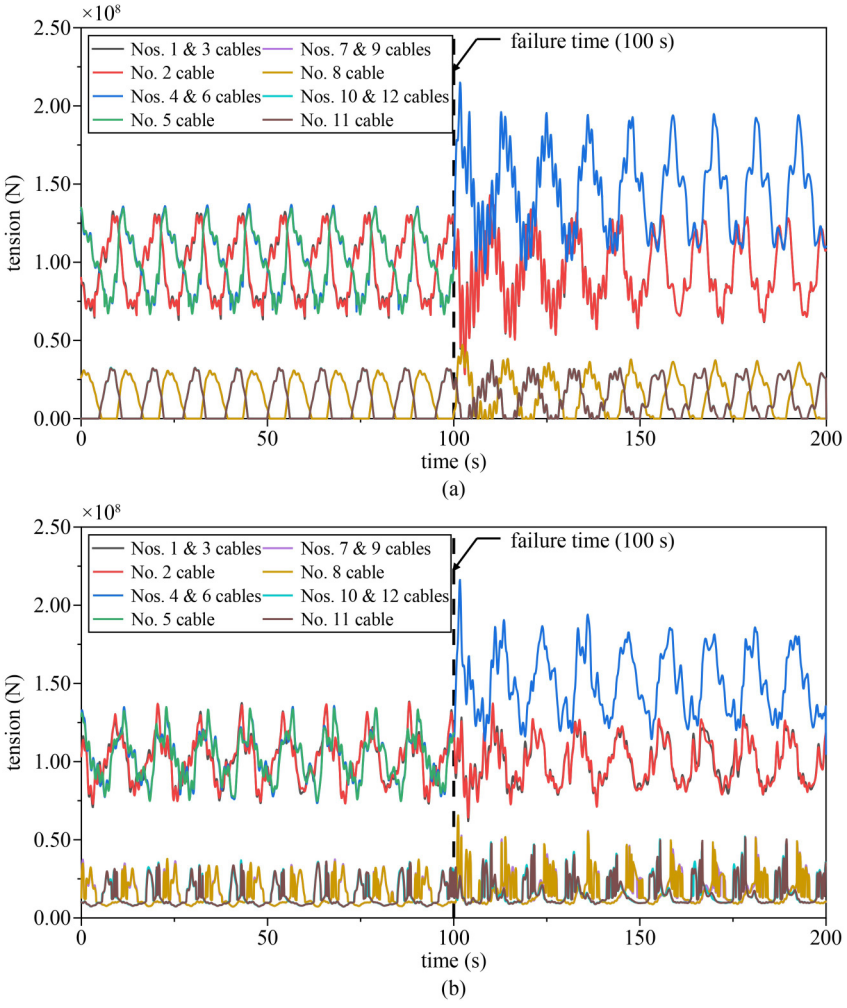

Fig. 11 Tension comparison of anchor cables with different mooring styles under No. 5 cable failure. (a) Mooring style 2; (b) mooring style 3.

1.1 s, current velocity = 0.1 m/s, and BWR = 1.5), the sway motions and cable tensions of the SFT for three mooring styles under cable failure were investigated (Figs. 12–14).

Prior to cable failure, the maximum amplitude of the sway motion for mooring styles 2 and 3 were much lower than that for mooring style 1 (see Fig. 12). This observation implies that mooring styles 2 and 3 offer better vibration suppression ability than mooring style 1. After the cable failed, the sway motions of the tube increased abruptly and the transient effect overshoot in mooring styles 1−3 were 2.86, 0.97, and 0.33 mm, respectively. Under a single anchor cable failure, the transient response of the tube for the SFT was weak owing to the compliance of the motion in the sway direction. In addition, because of cable failure, the new equilibrium position of the tube for mooring style 1 shifted more significantly than that of the other mooring styles.

Figure 13 shows the time histories of the No. 4 cable tension of the SFT under No. 5 cable failure for different mooring styles. Prior to cable failure, the descending order of tension amplitudes for the three mooring styles was mooring styles 1, 3, and 2. After the cable failed, all the tension amplitudes of the three mooring styles increased significantly and then stabilized at a high tension level, particularly in mooring styles 1 and 2. The amplitude of the variation in the tension and convergence time of mooring style 1 was larger than that of mooring styles 2 and 3. Additionally, some distinct perturbations in post-failure tension were observed in mooring styles 1 and 2. Moreover, after the cable failed, the variation in the tension was more significant than that in the tube motion, as shown in Fig. 12. This implies that, the risk of mooring failure in the remaining cables and the subsequent progressive failure of the SFT are more severe than the risk of stability loss of the tube.

Figure 14 shows the maximum tensions of the cables for the SFT with and without No. 5 cable failure for different mooring styles. In this section, the coefficient of variation is introduced to evaluate the uniformity of the cable tensions along the SFT under different mooring

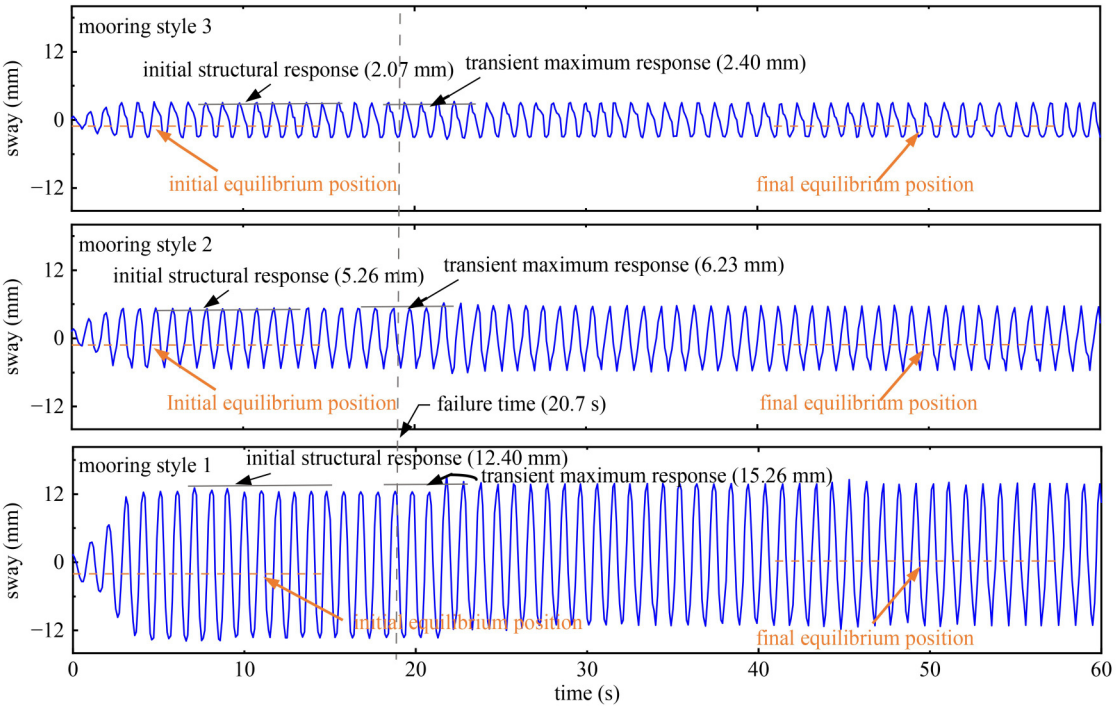

Fig. 12 Time history of sway motion of tube under No. 5 cable failure for different mooring styles.

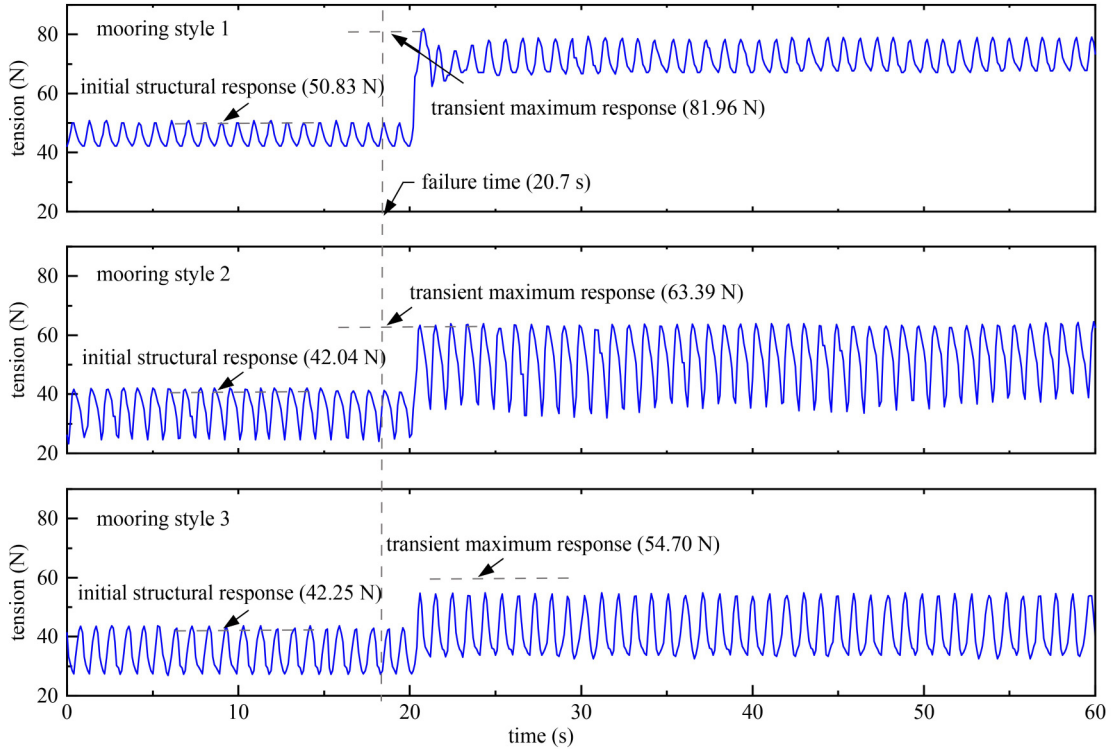

Fig. 13 Time history of tension of No. 4 cable for SFT under No. 5 cable failure for different mooring styles.

styles. Here, this coefficient is expressed as the ratio of the standard deviation to the mean value. Prior to cable failure, the coefficient of variation for mooring style 1 was 0.00323, which is lower than those for mooring styles 2 and 3. This implies that the cable tensions of mooring style 1 were the most uniform among the three mooring styles. However, the average cable tension of mooring style 1 was 51.2 N, which was the largest among the mooring styles. Additionally, the effect of the cable failure on the remaining cable tension was significant for the different mooring styles. In this regard, the coefficients of variation for the mooring styles 1–3 were

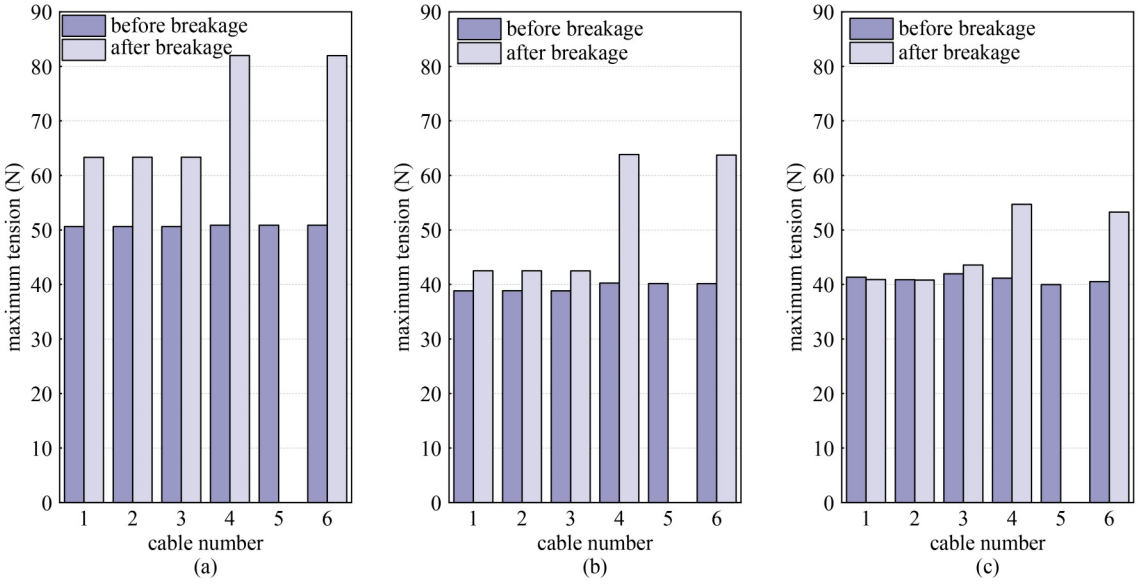

Fig. 14 Maximum tensions of cables for SFT before and after No. 5 cable failure for different mooring styles. (a) Mooring style 1; (b) mooring style 2; (c) mooring style 3.

0.71, 0.55, and 0.56, respectively, which implies that the uniformity of the cable tensions in mooring style 1 deteriorated due to the cable failure. Furthermore, the tensions of the remaining cables in mooring style 1 increased more significantly than that in mooring styles 2 and 3, particularly for the Nos. 4 and 6 cables, which were located at the same side of the broken cable. This indicates that, under cable failure, mooring style 1 demonstrated the worst tension suppression among the three mooring styles.

5.2 Effects of key parameters on SFT performance

Based on previous studies [29,30], the dynamic coefficient (*DC*) is defined as the ratio of the dynamic response in the intact state before cable failure to the maximum structural response after cable failure, which is expressed as follows:

$$DC = \frac{\gamma}{\alpha}, \tag{1}$$

where α is the maximum structural response in the intact state before the anchor cable breaks, and γ is the maximum response of the remaining structures in the new equilibrium after the internal force is redistributed.

The *DC* is primarily used to evaluate the effect of cable breakage on the sensitivity of the structure under abrupt loading excitation variations.

5.2.1 Effect of wave period

Figure 15 shows the maximum motion amplitudes and *DC* of the tube under No. 5 cable failure for different wave periods. Notably, the maximum motions in mooring style 1 were more significant than those in mooring styles 2 and 3. This might be because the mooring stiffness of mooring style 1 is significantly lower than that of mooring styles 2 and 3, which implies that the tension change of the anchor cables in mooring style 1 is extremely sensitive to cable failure. Furthermore, this result indicates that after an abrupt failure of the cable, mooring style 1 demonstrates the worst vibration suppression ability. The *DC* curves based on the sway motion of the three mooring styles show significant fluctuations and irregularities. Moreover, the *DC* based on the sway motion of mooring style 3 was much larger than that of the other mooring styles. The *DC* curve characteristics of the three mooring styles were similar to the curves of the maximum heave motion. As the wave period increased, the *DC* for mooring style 1 increased and then decreased, whereas the peak period shifted to the wave period of 0.7 s. This is attributable to the decrease in the mooring stiffness of the SFT due to cable failure as well as the variance in the systemic natural period, which results in variations in the dynamic behavior of the SFT. The evaluation factors for the maximum heave motion and *DC* of the SFT are related to some extent. The maximum heave motion occurred when the period was 1.3 s, whereas the maximum value for the dynamic amplification coefficient was indicated when the period was 0.7 s, as shown in Fig. 15(b).

Figure 16 shows the effects of the wave periods on the maximum amplitude and *DC* of tension of the No. 4 cable due to No. 5 cable failure. Based on observation, the tension values for mooring style 1 were much higher than those for mooring styles 2 and 3. The trends of the maximum tension curves for mooring styles 2 and 3 were

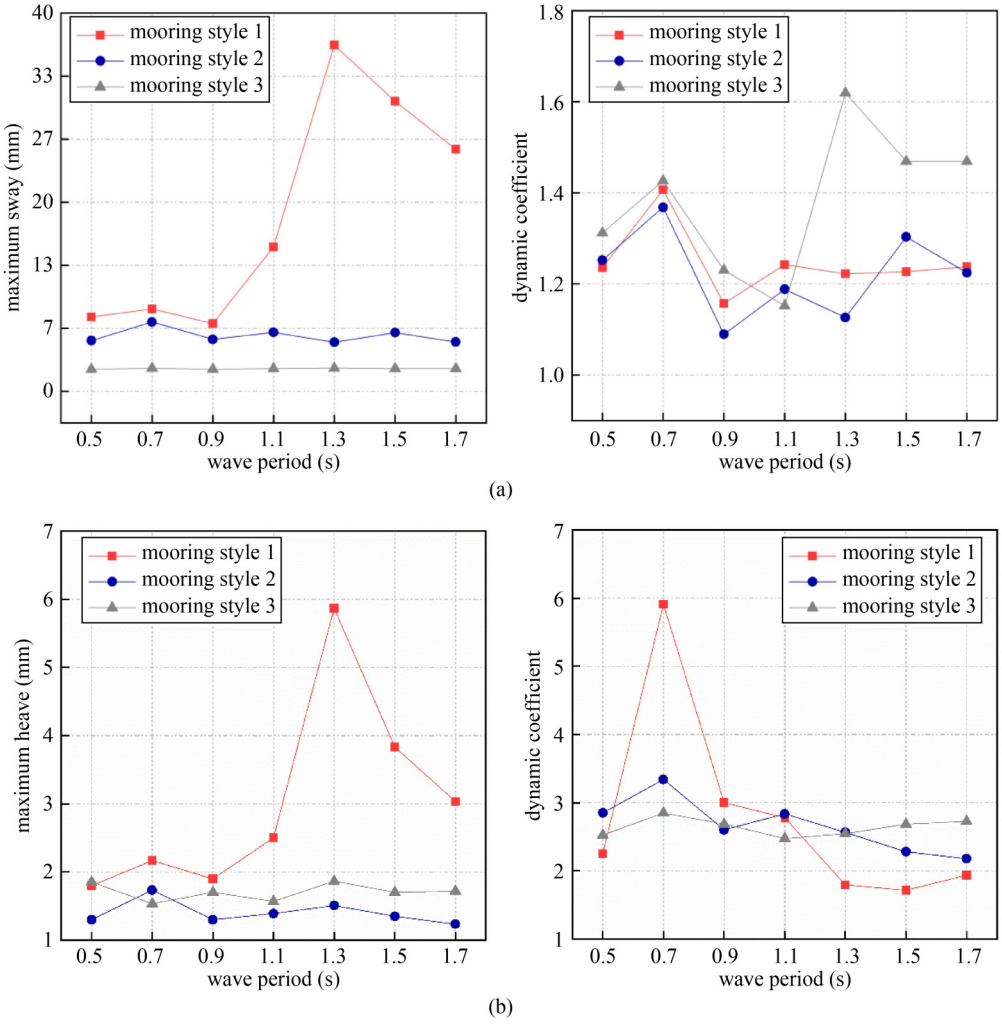

Fig. 15 Maximum motion amplitudes and *DC* of tube under No. 5 cable failure for different wave periods. (a) Sway; (b) heave.

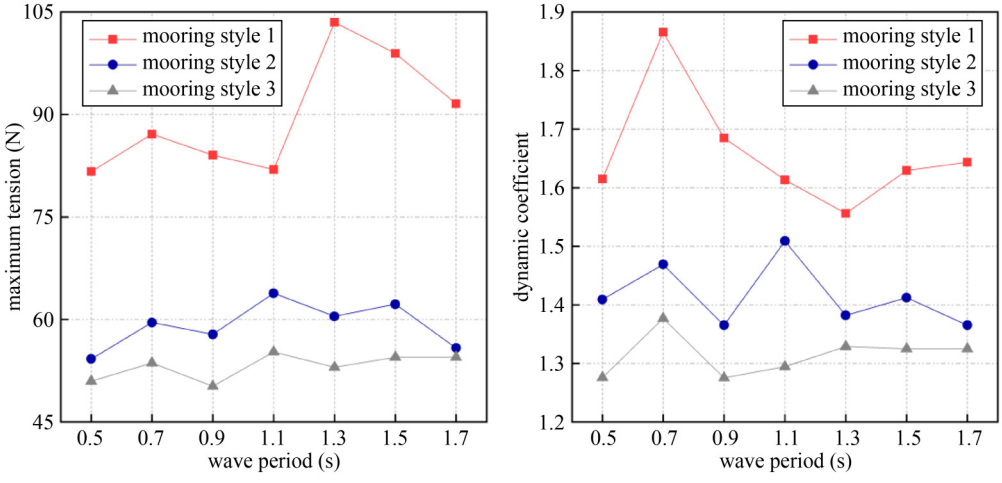

Fig. 16 Maximum amplitude and *DC* of tension of No. 4 cable under No. 5 cable failure for different wave periods.

similar. The *DC* of the tension after cable failure for the three mooring styles was between 1.28 and 1.87. Among the three mooring styles, the *DC* of the tension in mooring style 1 was the highest, which appeared at the wave period of 0.7 s, followed by those in mooring styles 2 and 3.

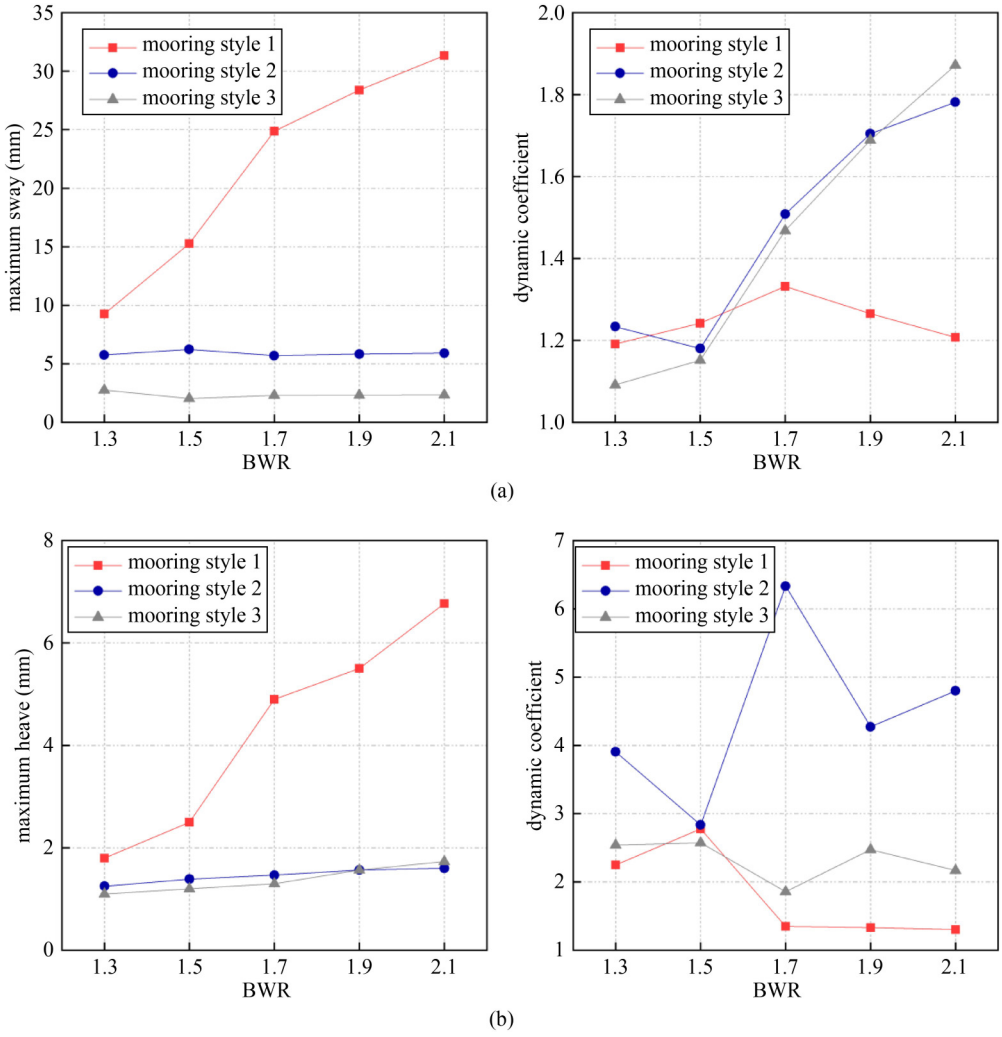

Fig. 17 Maximum motion amplitudes and *DC* of tube under No. 5 cable failure for different BWRs. (a) Sway; (b) heave.

5.2.2 Effect of BWR

As shown in Fig. 17(a), when the BWR increased (after cable failure), the sway motion of the tube in mooring style 1 increased significantly; by contrast, the sway motions in mooring styles 2 and 3 remained unchanged in general, The sway motion in mooring style 1 was greater than those in mooring styles 2 and 3, particularly at BWRs of 1.7–2.1. The *DC*s of the sway motion for the three mooring styles generally increased with the BWR, except for that of mooring style 1 (BWR = 1.7–2.1). This implies that under cable breakage, as the BWR increases, the failure risk of the remaining cables and the stationarity and safety loss of the tube increase.

Additionally, the heave motion after cable failure in the three mooring styles increased with the BWR (Fig. 17(b)). Notably, the amplitude variation of mooring style 1 was significant. For the *DC*s of heave motion, the three curves generally exhibited significant fluctuations and randomness. The curve of mooring style 2 was much larger than those of the other mooring styles, which may be due to the insignificant heave response in mooring style 2 prior to cable failure.

The maximum tension after cable failure for all mooring styles increased with the BWR (Fig. 18). Compared with the values of mooring styles 2 and 3, the maximum tension under cable failure in mooring style 1 was greater. The aforementioned results indicate that, after cable failure, the burden of the remaining cables is increased by larger BWRs, which will further increase the failure risk of the remaining cables and the progressive failure of the entire SFT. The maximum tension of the three mooring styles increased until a BWR of 1.5, after which the tension decreased.

5.3 Progressive failure of remaining structure

In the most extreme cases, progressive failure can occur under certain circumstances involving cable failure. To investigate the failure mechanism of the SFT under the

three mooring styles, the cable failure mode (the breaking tensions of all the cables were reduced to 75 N, and cable No. 5 was first triggered to break at 30 s) was induced to trigger a progressive failure. For simplicity, the restraint condition of both ends of the tube was assumed to be free in the progressive failure investigation. The tube traces and experimental observations of the segmental model for the three mooring styles are shown in Figs. 19 and 20, respectively.

As shown in Fig. 19(a), prior to cable failure, the tube in mooring style 1 shifted slightly but regularly in the vicinity of the initial balance position. Once the cable failed, because the mooring constraint was loosened considerably, the tube motion trace diverged and elevated significantly toward the water surface and showed more random and unstable characteristics. After the elevation, the tube was positioned at a new equilibrium position around the waterline. The average drift displacements in the vertical and horizontal directions were 225.6 and 110.2 mm, respectively. After cable failure, the tube trace in mooring style 2 did not change significantly and diverged only slightly (Fig. 19(b)). Meanwhile, the tube trace in mooring style 3 exhibited a high degree of consistency between the normal and broken cases (Fig. 19(c)). The results above indicate that, with sufficient tension burden redundancy by the remaining anchor cables, cable failure does not trigger progressive failure in the SFT with mooring styles 2 and 3. Specifically, the SFT with mooring style 3 exhibited the highest resistance to progressive failure.

Figure 20 shows the experimentally observed SFT motion for the three mooring styles during the entire process. Figures 20(a)–20(c) and 20(d)–20(f) show the detailed observations of SFT motion for mooring style 1 before and after cable failure, respectively. From 0.0 to 30.0 s, the tube moves steadily and regularly around the initial position before the cable failed; subsequently, it failed progressively. Figure 20(c) shows the tube motion when the No. 5 cable was broken at 30.0 s, i.e., the motion of the tube varied slightly. However, because of the failure of the No. 5 cable, the tension redistribution and impact force due to the failure might affect the

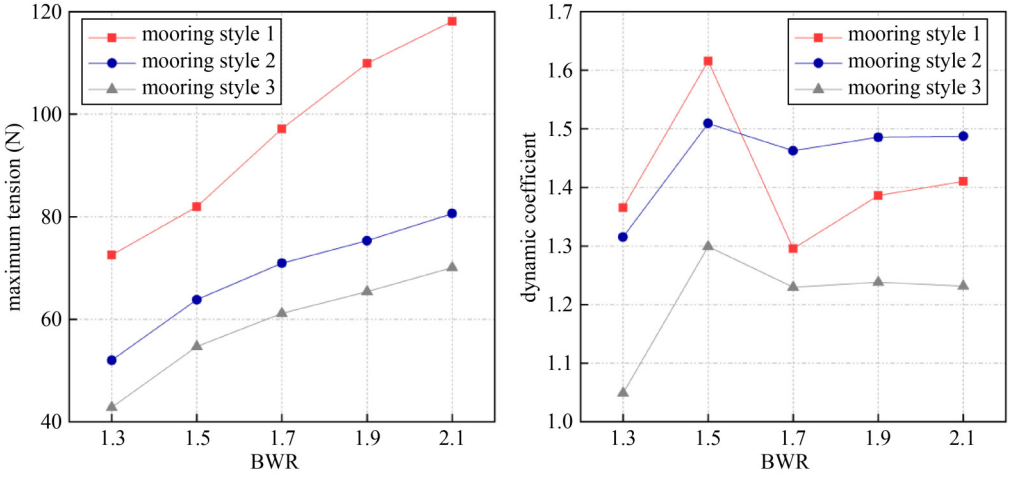

Fig. 18 Maximum tension and *DC* of No. 4 cable under No. 5 cable failure for different BWRs.

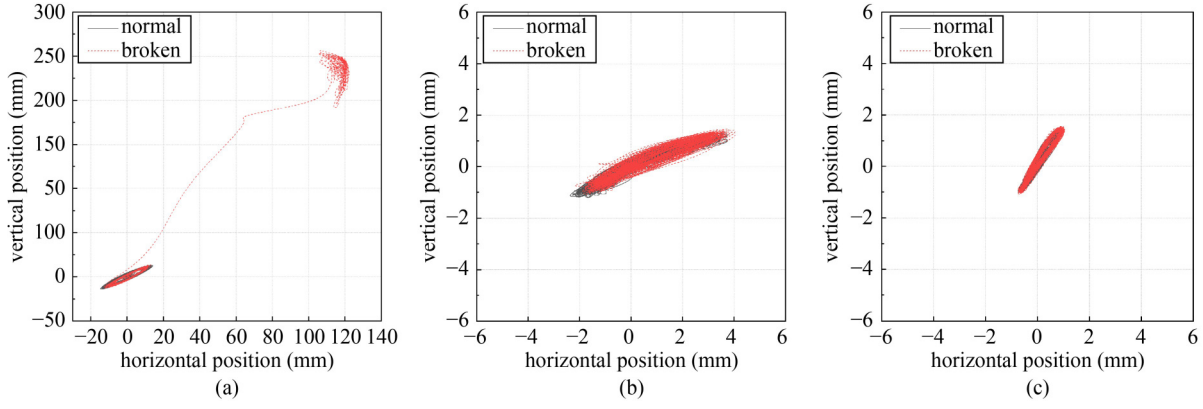

Fig. 19 Traces of segmental model for different mooring styles under No. 5 cable failure (cable-failure force = 75 N). (a) Mooring style 1; (b) mooring style 2; (c) mooring style 3.

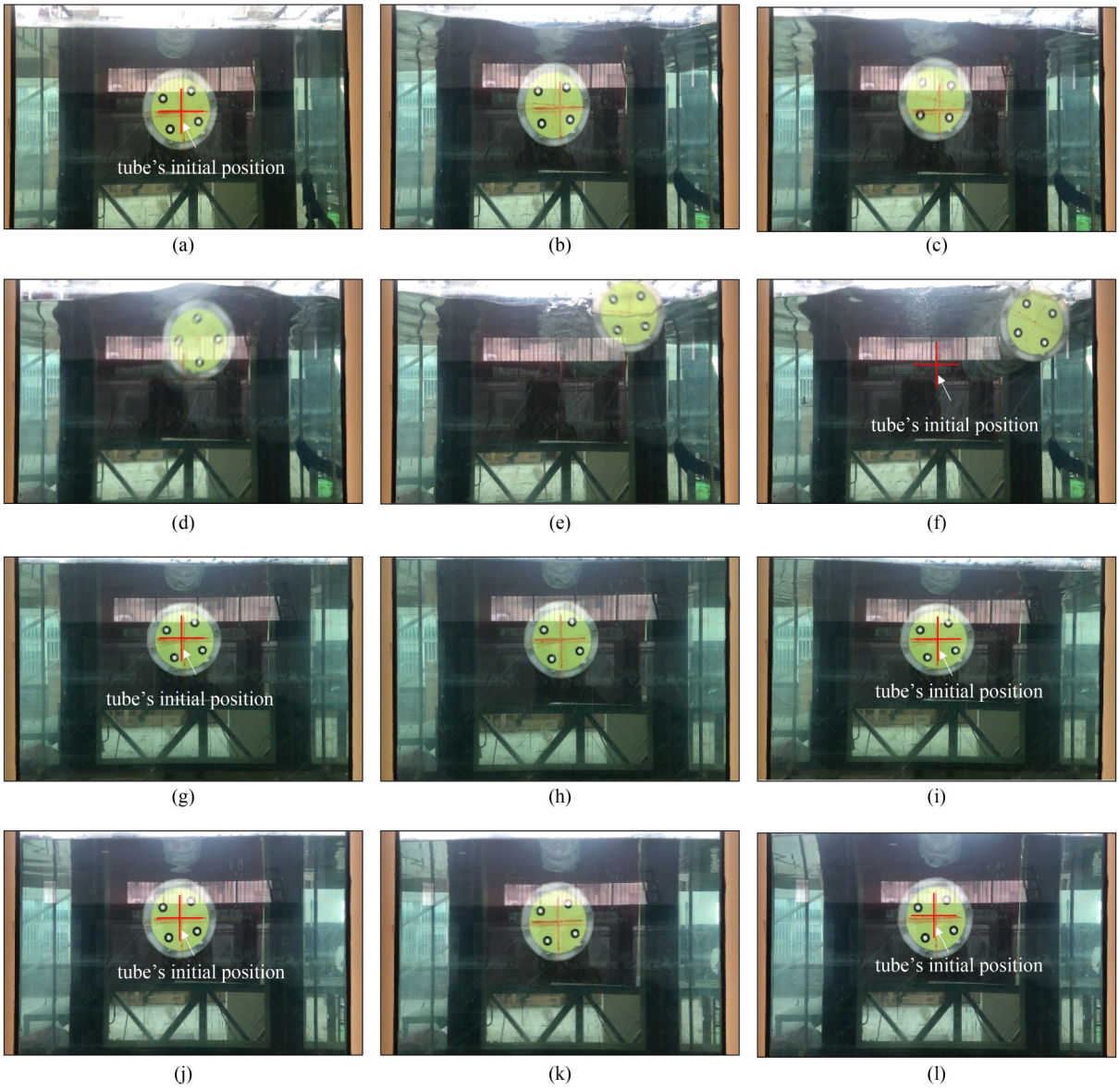

Fig. 20 Experimental observation for SFT motion with different mooring styles under No. 5 cable failure (cable-failure force = 75 N). (a) Mooring style 1, t = 0.0 s; (b) mooring style 1, t = 15.0 s; (c) mooring style 1, t = 30.0 s; (d) mooring style 1, t = 30.5 s; (e) mooring style 1, t = 31.0 s; (f) mooring style 1, t = 32.0 s; (g) mooring style 2, t = 0.0 s; (h) mooring style 2, t = 30.0 s; (i) mooring style 2, t = 32.0 s; (j) mooring style 3, t = 0.0 s; (k) mooring style 3, t = 30.0 s; (l) mooring style 3, t = 32.0 s.

remaining cables. In particular, the tensions of the remaining cables increased rapidly and reached the presupposed threshold value, which resulted in the failure of the other cable after approximately 0.5 s, as shown in Fig. 20(d). The equilibrium state and stability of the SFT were lost, whereas the front end of the tube was elevated and rolled rapidly toward the water surface, as shown in Figs. 20(e) and 20(f). Finally, the SFT was in an unsteady equilibrium state under the constraint of the remaining cables and floated at the water surface at a position distant from the initial position, which implies the progressive failure of the entire SFT. The total duration of the progressive failure was approximately 5 s. This process occurred abruptly and rapidly, which does not facilitate engineering prediction and disposition. In addition, the SFT motion with mooring styles 2 and 3 after cable failure did not indicate significant changes (Figs. 20(g)–20(i) and Figs. 20(j)–20(l)).

6 Results and discussions of entire-length numerical model

For field applications, the hydrodynamic behavior and progressive failure mechanism of an entire-length SFT model under cable failure must be investigated more closely. Owing to the restriction of the wave–current flume, the test for the entire-length model was difficult to

perform in this study. In this study, an entire-length numerical model based on the three mooring styles was established to perform the abovementioned investigation. Based on an entire-length numerical model with mooring style 1 as an example, 13 pairs of cables were arranged along the outside of the SFT, which were numbered 1–26, where Nos.1–13 and 14–26 were arranged at the downstream and upstream sides, respectively (Fig. 21). Similarly, for mooring styles 2 and 3, the outside cables were numbered 1–26.

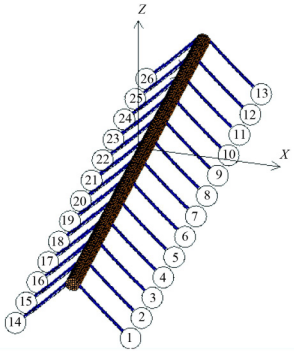

Fig. 21 Entire-length SFT model for mooring style 1.

6.1 Dynamic analysis for a typical calculation case

In this section, only the sway and heave motion of the tube and the tension of the typical cables are considered under the combined action of waves and currents (wave height = 2.5 m, wave period = 10 s, and current velocity = 1.2 m/s). The typical time histories of 1) the motion responses of the tube and 2) the tension of the typical cables under No. 20 cable failure are shown in Figs. 22 and 23, respectively. To provide clearer results, the time series from 150 to 250 s is enlarged.

After cable failure, the sway motion curve for the three mooring styles did not change significantly (Fig. 22(a)). However, a slight transient amplification of the motion amplitude was observed. In mooring style 3, the sway motion of the tube exhibited multiple frequencies prior to cable failure. This phenomenon is likely caused by the coupled interaction between the tube and its inner crossover cables. After the cable failed, this characteristic diminished and a new curve was exhibited, which reached a new equilibrium within 6 s. Meanwhile, the transient heave motions of the three mooring styles with cable failure were more significant than the transient sway motion (Fig. 22(b)). This is because the heave motion of the SFT was easily constrained by the anchor cable under the tension state as compared with the sway motion. Under cable failure, the transient motion with a larger loss amplitude of rigidity in the heave motion increased. The variation amplitudes of the heave motion for the mooring styles 1–3 were 4.18, 2.75, and 3.62 mm, respectively. Before and after cable failure, mooring style

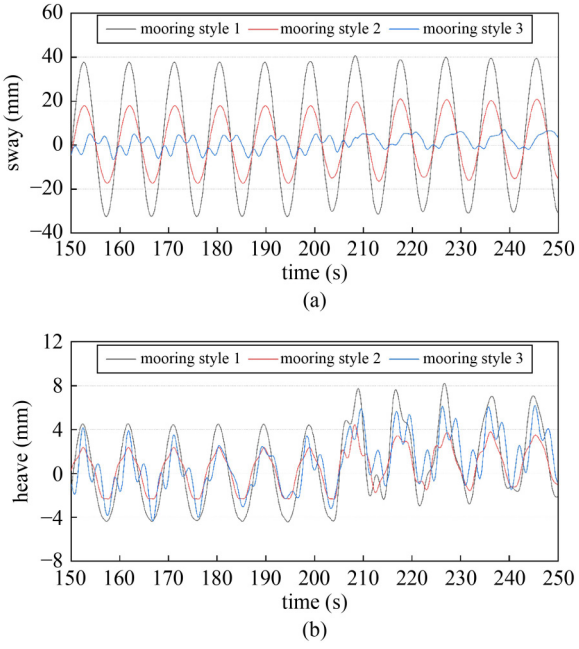

Fig. 22 Time history of motion responses of tube under No. 20 cable failure. (a) Sway; (b) heave.

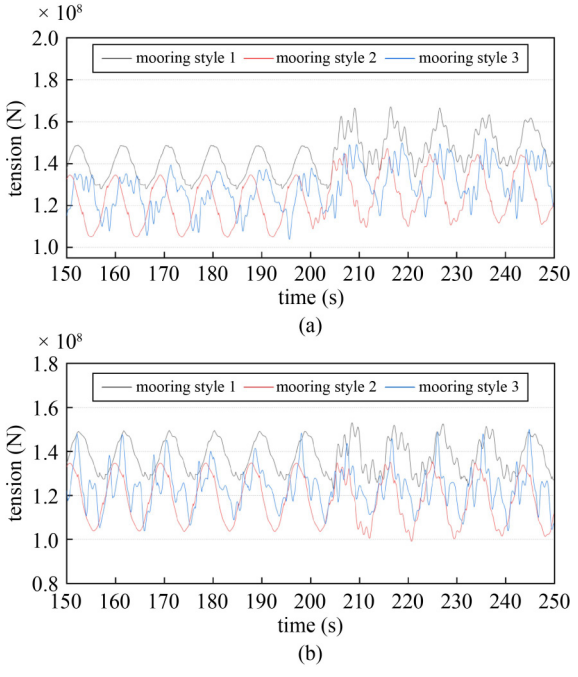

Fig. 23 Time history of tension of typical remaining cables under No. 20 cable failure. (a) No. 21 cable; (b) No. 7 cable.

3 demonstrated the best vibration suppression ability for the SFT among all the mooring styles.

After cable failure, the tension of the No. 21 cable (near broken cable No. 20 at the same side) for the three mooring styles increased significantly (Fig. 23(a)). In particular, the tension variation amplitudes of the No. 21 cable for mooring styles 1–3 were 1.82×10^7, 1.02×10^7,

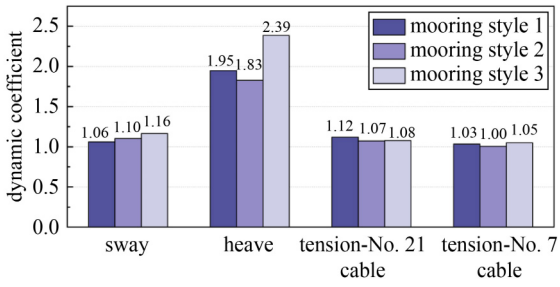

Fig. 24 *DC*s of motion amplitude and cable tension under No. 20 cable failure.

and 1.10×10^7 N, respectively. The tension variation of the No. 7 cable (at the offside of broken cable No. 20) with different mooring styles was insignificant, particularly for mooring styles 2 and 3 (Fig. 23(b)).

Figure 24 shows the *DC*s of the tube motions and cable tensions for the three mooring styles under No. 20 cable failure. The result shows that the *DC* of the heave motion is larger than that of the sway motion. This implies that the heave motion is more sensitive and thus more dangerous under cable failure. Among all the mooring styles, mooring style 3 indicated the largest *DC* for the motions, particularly for the heave motion, whose *DC* was 2.39. Therefore, mooring style 3 demonstrates the best vibration suppression ability for the SFT but the worst sensitivity for motion under cable failure. Meanwhile, the *DC*s of the tensions were relatively small, i.e., between 1.00 and 1.12. In general, the change in the tube motion caused by cable failure is significant, whereas the change in the cable tension caused by cable failure is insignificant.

6.2 Effect of cable failure mechanism

Multiple cable failures can occur in a complex marine environment, thus jeopardizing the security and stationarity of SFTs. Thus, to investigate the hydrodynamic behavior of an SFT under multiple cable failure events, three different cable failure methods were selected, as shown in Table 5. The *DC*s of the sway and heave motions for the aforementioned three cable failure mechanism based on a wave height of 2.5 m, wave period of 10 s, and current velocity of 1.2 m/s are shown in Figs. 25(a) and 25(b).

Table 5 Three different cable failure mechanisms

Case No.	positions of cable failure
1	19, 20, 21
2	7, 19, 20
3	6, 7, 19, 20

Compared with the *DC*s of the other cases, the *DC* of the sway motion under Case 3 (four broken cables set

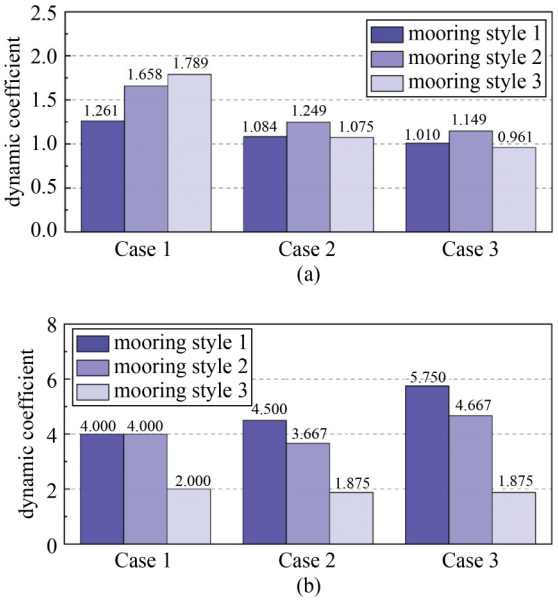

Fig. 25 *DC*s of motion amplitude and cable tension of SFT under different cable-failure cases. (a) Sway; (b) heave.

symmetrically on both sides) were the smallest; in fact, it was smaller than that of the single cable failure (Fig. 24). This implies that more broken cables do not necessarily correspond to a more significant variation of the SFT under cable failure, as the distribution of broken cables is a contributing factor as well. Specifically, the SFT reforms a symmetric mooring system along the *Y*-axis under Case 3 after the failure of four symmetric anchor cables, i.e., after the SFT is stabilized under a failure scenario, the equilibrium position of the SFT remains the same as that from the pre-failure state. Meanwhile, in asymmetric cases, the equilibrium position of the tube of SFT under an asymmetric anchor cable failure shift to the side with more remaining anchor cables. Conversely, the *DC* in the heave motion under the Case 3 is larger than that of the other cases. These results indicate that symmetric cable failures can result in significant disturbance in the heave motion but less disturbance in the sway motion. Moreover, for all mooring styles, the *DC* of the heave motion is generally much larger than that of the sway motion, which implies that the risk of the abruptly increasing instability in the heave motion under cable failure is higher than that in the sway motion. Based on the results, mooring style 3 indicates better ability in maintaining the stationarity of the SFT under cable failure, as compared with the other mooring styles, except for the sway motion in Case 1.

6.3 Progressive failure of remaining structure

Although SFTs are typically designed with sufficient structural redundancy, extreme environmental excitations (earthquakes and tsunamis) may induce cable failure

abruptly, which may cause progressive failures, such as zipper-like collapse [31]. Based on the aforementioned results, the transient effect, the redistribution of forces, and the impact force of the SFT after cable failure under different situations are key for determining the occurrence of progressive failure. To investigate the progressive failure mechanism of the entire-length model under the three mooring styles, a specific cable failure method (where the cable failure tension of the cables is reduced to 2.338×10^8 N using the cable failure method of Case 1) for triggering progressive failure is proposed herein.

Figure 26 shows the traces of the entire-length numerical model for the three mooring styles after cable failure under different wave conditions, as in the typical cable failure case (cable-failure force = 2.338×10^8 N). As the wave height increased, the tube traces after cable failure for mooring styles 2 and 3 indicated larger and more irregular fluctuations, although stability was maintained. The tube finally reached a new equilibrium position at the vicinity of the original point while its size increased proportionally. For mooring style 1, when the wave height was small (wave height = 1 and 2 m), the tube motion after cable failure became divergent and unstable; meanwhile, when the wave height was larger (wave height = 3 m), the tube trace after cable failure diverged and elevated significantly until the tube reached a new equilibrium position around the waterline, which signifies the progressive failure of the entire SFT. Additionally, owing to the complicated interaction between the SFT and wave–current flume under cable failure, the traces of the SFT typically indicated significant fluctuations and randomness. Consequently, the divergence and progressive failure of the SFT under cable failure became more conspicuous.

7 Conclusions

In this study, the dynamic behavior of an SFT with

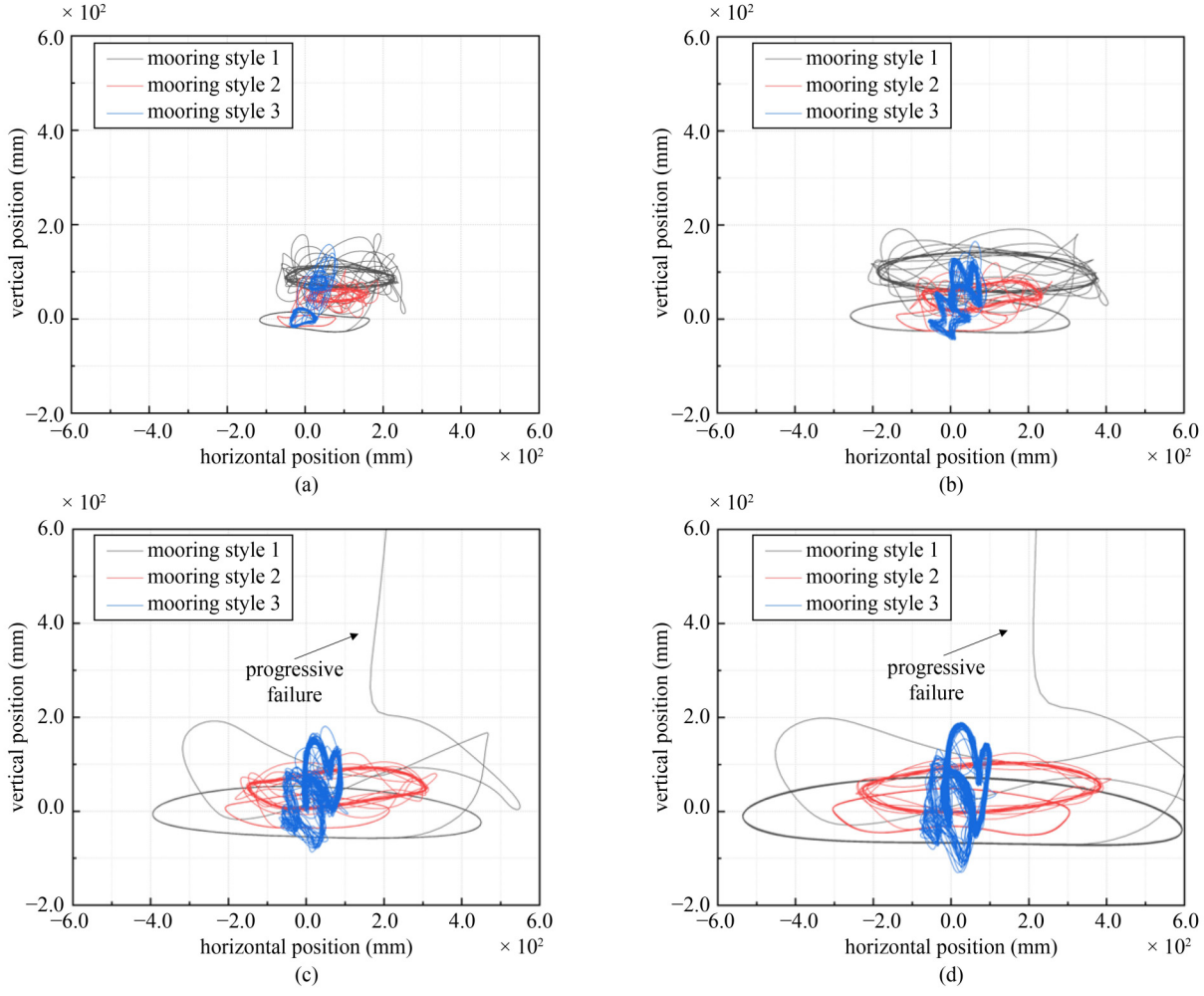

Fig. 26 Traces of entire-length SFT model for different mooring styles under different wave conditions. (a) Wave height = 1 m; wave period = 10 s; (b) wave height = 2 m; wave period = 10 s; (c) wave height = 3 m; wave period = 10 s; (d) wave height = 4 m; wave period = 10 s.

different mooring styles under local cable failure was investigated via model tests and numerical simulations. The conclusions are summarized below, and some engineering recommendations are provided.

1) An innovative analytical method and technology to investigate the dynamic behavior of an SFT with different mooring styles under cable failure was presented. For this investigation, a segment test, numerical models, and an entire-length numerical model were established. The numerical values obtained were consistent with the experimental results. The methods and models presented herein are applicable for investigating the dynamic performance and progressive failure behavior of SFTs under cable failure accurately.

2) The results of this study indicate that after cable failure, mooring style 1 demonstrated the worst vibration suppression ability, the most significant transient effect, and the highest tension level compared with the other mooring styles. Mooring styles 2 and 3 demonstrated the best vibration suppression ability in heave and sway motions, respectively, when cable failure occurred. However, when considering the engineering benefits, mooring style 1 is more economical than the other mooring styles. The abovementioned results should be considered comprehensively in the practical design of the SFT mooring style.

3) The hydrodynamic response of an SFT with different mooring styles under cable failure was comprehensively investigated using different key parameters, such as the wave period, BWR, and cable failure mechanisms. Based on the results, some recommendations were suggested for creating primary guidelines for the design, testing, and installation of SFTs to ensure that the abrupt failure of cables will not cause structural instability.

4) In engineering practice, cable tension with structural symmetry and uniformity are recommended to effectively prevent the formation of force concentration and avulsion mouth caused by cable failure. The robustness and resistance to progressive failure should be strengthened to eliminate the zipper-like collapse of SFTs. For the design of SFTs, the abrupt failure of one or more cables should not cause structural instability, and a corresponding "cable loss" load case was specified. This ensures that the zipper-like collapse initiated by cable failure and the overloading and failure of adjacent cables can be prevented.

5) The main focus of this study was the safety of SFTs under cable failure, whereas the stability of driving was not investigated and analyzed comprehensively. However, the driving stability might be affected significantly by the cable failure of the SFT during its service life. Robustness is widely recognized as an effective evaluation indicator for investigating the stability of a structure. Thus, a robustness analysis for assessing the driving stability of SFTs under cable failure should be conducted in the future.

Acknowledgements This study was supported by the National Natural Science Foundation of China (Grant Nos. 52268061, 51808136, and 51878185), China Scholarship Council (No. 201906660001), Guangxi Science and Technology Base and Talent Special Funds (No. 2019AC20264), and Guangxi Natural Science Foundation (No. 2018JJB160058).

Conflict of Interests The authors declare that they have no conflict of interest.

References

1. Jiang B, Liang B, Wu S. Feasibility study on the submerged floating tunnel in Qiongzhou strait, China. Polish Maritime Research, 2018, 25(s2): 4−11
2. Minoretti A, Xiang X, Johansen I, Eidem M. The future of the tunnel crossing: The submerged floating tube bridge. Structural Engineering International, 2020, 30(4): 493−497
3. Dong M, Miao G, Yong L, Niu Z, Pang H, Hou C. Effect of escape device for Submerged Floating Tunnel (SFT) on hydrodynamic loads applied to SFT. Journal of Hydrodynamics, 2012, 24(4): 609−616
4. Zhang H, Yang Z, Li J, Yuan C, Xie M, Yang H, Yin H. A global review for the hydrodynamic response investigation method of submerged floating tunnels. Ocean Engineering, 2021, 225: 108825
5. Lu W, Ge F, Wu X, Hong Y. Nonlinear dynamics of a submerged floating moored structure by incremental harmonic balance method with FFT. Marine Structures, 2013, 31: 63−81
6. Seo S, Mun H, Lee J, Kim J. Simplified analysis for estimation of the behavior of a submerged floating tunnel in waves and experimental verification. Marine Structures, 2015, 44: 142−158
7. Cantero D, Ronnquist A, Naess A. Tension during parametric excitation in submerged vertical taut tethers. Applied Ocean Research, 2017, 65: 279−289
8. Naik M, Zahid U, Dong-Ho C. Performance evaluation of submerged floating tunnel subjected to hydrodynamic and seismic excitations. Applied Sciences, 2017, 7(11): 1−17
9. Luo G, Pan S, Zhang Y, Ren Y, Xiong K. Displacement response of submerged floating tunnel with flexible boundary under explosion load. Advances in Structural Engineering, 2021, 24(2):

346−358
10. Chen X, Chen Q, Chen Z, Cai S, Zhuo X, Lv J. Numerical modeling of the interaction between submerged floating tunnel and surface waves. Ocean Engineering, 2021, 220: 108494
11. Xie J, Chen J. Dynamic response analysis of submerged floating tunnel-canyon water system under earthquakes. Applied Mathematical Modelling, 2021, 94: 757−779
12. Lee J, Jin C, Kim M. Dynamic response analysis of submerged floating tunnels by wave and seismic excitations. Ocean Systems Engineering, 2017, 7(1): 1−19
13. Liu Y, Jin R, Geng B, Zhang H, Ren C. Influence of anchor cable inclination angle on motion response of submerged floating tunnel with different section. Chinese Journal of Hydrodynamics, 2020, 35(2): 237−247 (in Chinese)
14. Xiang Y, Chen Z, Bai B, Lin H, Yang Y. Mechanical behaviors and experimental study of submerged floating tunnel subjected to local anchor-cable failure. Engineering Structures, 2020, 212: 110521
15. Zhou Y, Chen S. Numerical investigation of cable breakage events on long-span cable-stayed bridges under stochastic traffic and wind. Engineering Structures, 2015, 105: 299−315
16. Minaei A, Daneshjoo F, Goicolea J. Experimental and numerical study on cable breakage equivalent force in cable-stayed structures consisting of low-relaxation seven-wire steel strands. Structures, 2020, 27: 595−606
17. Wu G, Qiu W, Wu T. Nonlinear dynamic analysis of the self-anchored suspension bridge subjected to sudden breakage of a hanger. Engineering Failure Analysis, 2019, 97: 701−717
18. Bae Y, Kim M, Kim H. Performance changes of a floating offshore wind turbine with broken mooring line. Renewable Energy, 2017, 101: 364−375
19. Jakobsen B. Design of the submerged floating tunnel operating under various conditions. Procedia Engineering, 2010, 4: 71−79
20. Wu Z, Wang D, Ke W, Qin Y, Lu F, Jiang M. Experimental investigation for the dynamic behavior of submerged floating tunnel subjected to the combined action of earthquake, wave and current. Ocean Engineering, 2021, 239(1): 109911
21. Wu Z, Yang S, Tang L, Ma H, Mou L, Xiao Y. Experimental investigation and analysis for hydrodynamic behaviours and progressive collapse phenomenon of submerged floating tunnel under anchor cables' breakage. Ships and Offshore Structures, 2022, 17(9): 1924−1938
22. Submerged Floating Tunnel Structural and Design Joint Team of Tackling Technological Problems. Submerged Floating Tunnel Engineering and Technology Research Introduction. Beijing: Science Press, 2019 (in Chinese)
23. Kanie S. Feasibility studies on various SFT in Japan and their technological evaluation. Procedia Engineering, 2010, 4: 13−20
24. Larssen R, Jakobsen S. Submerged floating tunnels for crossing of wide and deep fjords. Procedia Engineering, 2010, 4: 171−178
25. Yang Z, Huang B, Kang A, Zhu B, Han J, Yin R, Li X. Experimental study on the solitary wave-current interaction and the combined forces on a vertical cylinder. Ocean Engineering, 2021, 236: 109569
26. Chen J, Li J, Sun S, Su Z. Experimental and numerical analysis of submerged floating tunnel. Journal of Central South University, 2012, 19(10): 2949−2957
27. Lin W, Liu M, Zhou Z, Chen J, Yang Z, Zhang J. Relevant issues about real stiffness of submerged floating tunnel section-model. China Harbour Engineering, 2020, 40(2): 31−37 (in Chinese)
28. Morison J R, Johnson J W, Schaaf S A. The force exerted by surface waves on piles. Journal of Petroleum Technology, 1950, 2(5): 149−154
29. Wang X, Chen Z, Yu Y, Liu H. Numerical and experimental study on loaded suspendome subjected to sudden cable failure. Journal of Constructional Steel Research, 2017, 137: 358−371
30. Mozos C, Aparicio A. Numerical and experimental study on the interaction cable structure during the failure of a stay in a cable stayed bridge. Engineering Structures, 2011, 33(8): 2330−2341
31. Starossek U. Typology of progressive collapse. Engineering Structures, 2007, 29(9): 2302−2307